Ca^{2+} Regulation in the Na^+/Ca^{2+} Exchanger Involves Two Markedly Different Ca^{2+} Sensors

Mark Hilge,[1,2,*] Jan Aelen,[1] and Geerten W. Vuister[1]
[1] Department of Biophysical Chemistry
Institute for Molecules and Materials
Radboud University Nijmegen
Toernooiveld 1
6525 ED Nijmegen
The Netherlands

Summary

The plasma membrane Na^+/Ca^{2+} exchanger (NCX) is almost certainly the major Ca^{2+} extrusion mechanism in cardiac myocytes. Binding of Na^+ and Ca^{2+} ions to its large cytosolic loop regulates ion transport of the exchanger. We determined the solution structures of two Ca^{2+} binding domains (CBD1 and CBD2) that, together with an α-catenin-like domain (CLD), form the regulatory exchanger loop. CBD1 and CBD2 are very similar in the Ca^{2+} bound state and describe the Calx-β motif. Strikingly, in the absence of Ca^{2+}, the upper half of CBD1 unfolds while CBD2 maintains its structural integrity. Together with a 7-fold higher affinity for Ca^{2+}, this suggests that CBD1 is the primary Ca^{2+} sensor. Specific point mutations in either domain largely allow the interchange of their functionality and uncover the mechanism underlying Ca^{2+} sensing in NCX.

Introduction

Ca^{2+} is an ambivalent signal that is both essential and potentially dangerous for cell life. The accurate control of the spatio-temporal homeostasis of Ca^{2+} is thus vital and demands a regulatory machinery of exquisite precision and complexity (Carafoli, 2004). Ca^{2+} enters the cytoplasm through either the plasma membrane Ca^{2+} channels or the Ca^{2+} release channels of internal Ca^{2+} stores such as the endo/sarcoplasmic reticulum. Because the cytosolic concentration of Ca^{2+} needs to remain constant, the equivalent amount of imported Ca^{2+} has to be continuously removed from the cytoplasm. This is accomplished by a rich diversity of plasma membrane (PMCA) and sarcoplasmic reticulum (SERCA) Ca^{2+} ATPases, the mitochondrial Ca^{2+} uniporter (Kirichok et al., 2004), and the plasma membrane Na^+/Ca^{2+} exchanger (NCX). For reviews see Carafoli (2002) and Berridge et al. (2003).

Na^+/Ca^{2+} exchange is the dominant Ca^{2+} efflux mechanism across the plasma membrane that reestablishes resting levels of Ca^{2+} in the heart after muscle contraction (Egger and Niggli, 1999) and in neurons upon sensory stimulation (Wang et al., 2005). In its major transport mode, NCX exports one Ca^{2+} for the uptake of three Na^+ ions (Kang and Hilgemann, 2004) and undergoes 2500–

5000 turnovers per second and molecule (Hilgemann et al., 1991; Egger and Niggli, 1999). A biochemically derived topology model predicts nine transmembrane α helices (Iwamoto et al., 1999; Nicoll et al., 1999) and a large cytosolic loop of ~500 residues for NCX (Figure 1A). Binding of Ca^{2+} ions to sites located in the cytosolic loop generally activates the exchanger (Hilgemann, 1990; Hilgemann et al., 1992a; Matsuoka et al., 1993), whereas binding of Na^+ ions has been shown to deactivate NCX (Hilgemann, 1990; Hilgemann et al., 1992b). Residues 371–509 are reported to form a putative high-affinity Ca^{2+} binding domain (K_d ~140–400 nM; [Levitsky et al., 1994]) and appear to bind Ca^{2+} on a beat-to-beat basis during excitation-contraction coupling in cardiomyocytes (Ottolia et al., 2004).

NCXs are virtually ubiquitous, being found in organisms ranging from *C. elegans* to humans. Based on the presence of two highly conserved α repeat regions (Nicoll et al., 1996a) that are located in the transmembrane domain (TM), H^+/Ca^{2+} exchangers (CAX), cation/Ca^{2+} exchangers (YRBG and CCX), K^+-dependent Na^+/Ca^{2+} exchangers (NCKX), and NCXs constitute the cation/Ca^{2+} exchanger superfamily (Cai and Lytton, 2004). The four known mammalian NCX isoforms, NCX1 (Nicoll et al., 1990), NCX2 (Li et al., 1994), NCX3 (Nicoll et al., 1996b), and NCX4 (Marshall et al., 2005), display ~70% sequence identity and do not show striking functional differences (Iwamoto and Shigekawa, 1998; Linck et al., 1998). Whereas NCX1 is virtually omnipresent, NCX2 and NCX3 expression is limited to the brain and skeletal muscle (Lee et al., 1994; Nicoll et al., 1996b).

In cardiac NCX1, residues C-terminal of Lys569 constitute a variable, alternative splicing region (Figures 1A and 1B) that arises from different combinations of six small exons (labeled A–F). Whereas exons A and B are expressed in a mutually exclusive manner, cassette exons C, D, E, and F can be combined freely. In this pool, the AD variant, detected in brain, constitutes the shortest splice variant and the ACDEF form, found in heart and skeletal muscle, the longest (Kofuji et al., 1994; Lee et al., 1994; Quednau et al., 1997). Thus far, 17 tissue-specific splice variants of NCX1, but no splice variants for NCX2 and only very few for NCX3, have been reported (Quednau et al., 1997).

In order to explore Ca^{2+} regulation in the structurally entirely uncharacterized NCX, we determined the structures of two Ca^{2+} binding domains (CBD1 and CBD2) that are located in the large exchanger loop. The existence of a second Ca^{2+} binding domain (CBD2) was inferred by a sequence identity of 27% of residues 501–650 with CBD1 as well as the presence of two acidic segments, reported to be crucial for Ca^{2+} binding (Levitsky et al., 1994), at homologous positions. Both CBD1 and CBD2 undergo conformational changes upon binding of Ca^{2+} and look very similar in the Ca^{2+} bound form, whereas in the absence of Ca^{2+}, the domains show dramatic structural differences. Along with different Ca^{2+} affinities, the two distinct Ca^{2+} sensors may enable the exchanger to dynamically operate over a wide concentration range. Finally, the structures of CBD1 and CBD2 permit

*Correspondence: m.hilge@nki.nl
[2] Present address: Netherlands Cancer Institute, Department of Molecular Carcinogenesis, Plesmanlaan 121, 1066 CX Amsterdam, The Netherlands.
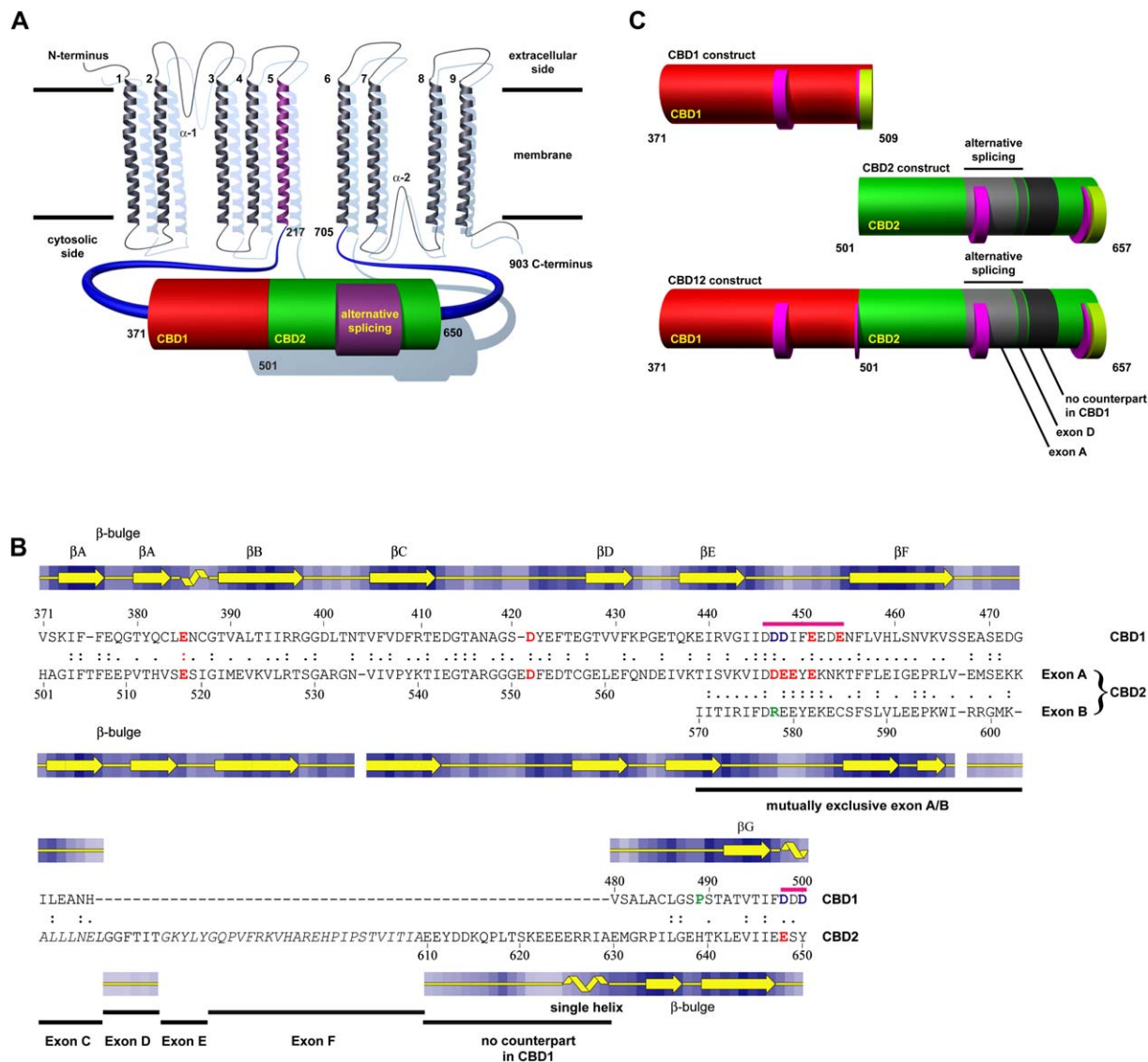
Figure 1. Overall Architecture of NCX and Constructs Used in This Study

(A) Topology model of NCX. The four NCX domains are depicted in unique colors: TM, gray; CLD, blue; CBD1, red; and CBD2, green. TM helix 5 and the region subjected to alternative splicing are displayed in violet. Boundaries of the domains are indicated by residue numbers and are based on the NCX1 AD-splice variant.

(B) Sequence alignment of CBD1 and CBD2. Double dots indicate identical residues and a single dot substitution by a similar residue. Dashes indicate inserts and italicized amino acids residues not taken into account for the numbering. Residues involved in Ca²⁺ binding are highlighted in red, whereas residues that are in addition mutation sensitive are shown in blue. The crucial arginine residue in exon B and the *cis* proline in CBD1 are highlighted in green. A pink bar above the letters indicates acidic segments. The secondary structure (yellow lines, arrows, and waves) and solvent accessibility in blue, as determined by PROCHECK-NMR (Laskowski et al., 1996), are shown above (CBD1) and below (CBD2) the alignment.

(C) Description of the constructs used in this study. All three constructs needed a C-terminal overhang (yellow regions) of seven to nine amino acids in order to bind Ca²⁺. Val371-Asp500 and His501-Tyr650 represent the Ca²⁺ binding domains CBD1 (red) and CBD2 (green), respectively. Pink regions display the acidic segments in the constructs. CBD2 contains a region subjected to alternative splicing. Regions in light gray and gray reflect exons A and D, whereas the region in dark gray symbolizes a CBD2 portion without counterpart in CBD1.

rationalization of an extensive body of biochemical and physiological data that have accumulated on regulation and modulation of NCX over the last two decades.

Results and Discussion

Structures of CBD1 and CBD2

We expressed three different constructs of canine NCX1 in *E. coli* BL-21 that encompassed residues 371–509, 501–657, and 371–657 (for construct details see Figure 1C), representing the stable forms of CBD1, CBD2, and CBD12, respectively. For CBD1 and CBD2, we determined the structures by high-resolution heteronuclear multidimensional NMR spectroscopy in the Ca²⁺ bound form. Both domains display the immunoglobulin fold that is, amongst others, also found in cadherins and fibronectins. The two antiparallel β sheets constitute a β sandwich or Greek key motif with one β sheet
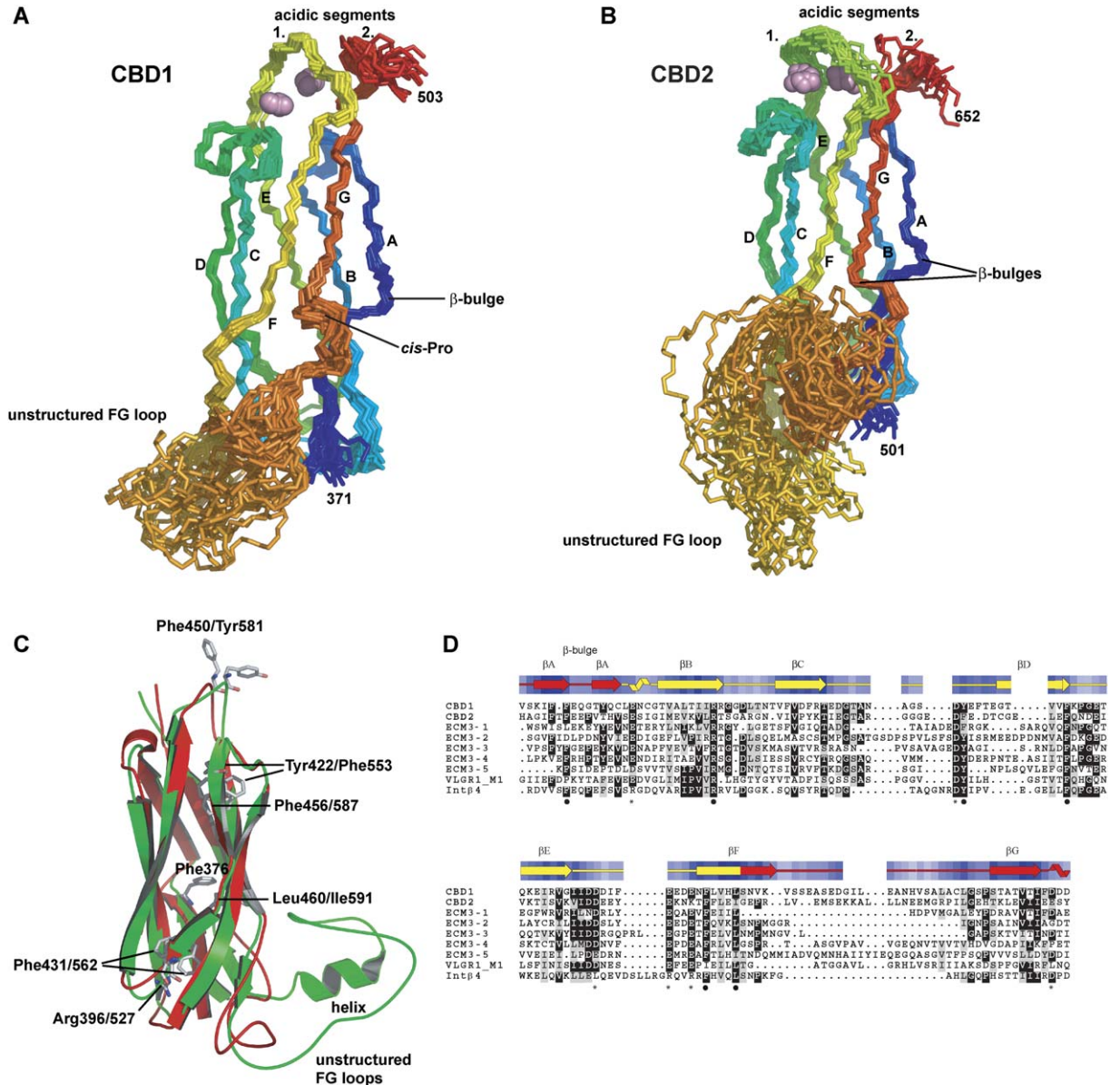
Figure 2. NMR Structures of the Exchanger Ca^{2+} Binding Domains and Redefinition of the Calx-β Motif

(A and B) Overlays of the 20 NMR-derived structures of CBD1 ([A], residues 371–509) and CBD2 ([B], residues 501–657) colored as a rainbow ramp ranging from blue (N terminus) to red (C terminus). Ca^{2+} ions are shown in pink. C-terminal residues 504–509 (CBD1) and 653–657 (CBD2) are disordered and removed from the figure for clarity.

(C) Ribbon diagram of the superposition of the central chains of CBD1 (red) and CBD2 (green). The orientation is ~180° rotated around the vertical axis with respect to the situation in (A) and (B). Residues discussed in the text are highlighted in ball-and-stick representation.

(D) Redefinition of the Calx-β motif. Sequence alignment of CBD1, CBD2, the five ECM3 Calx-β domains from sea urchin (EMBL accession code, AF287478), the first Calx-β domain in VLGR1 (EMBL accession code, AF055084), and the single Calx-β domain in integrin β4 (accession code, X51841). Conserved residues are highlighted black, whereas conservatively substituted residues are shaded gray. Conserved residues that coordinate Ca^{2+} in CBD1 and CBD2 are marked with an asterisk, whereas filled circles indicate structurally important residues. Secondary structure elements of CBD1 and CBD2 are displayed above the sequences with the original Calx-β motif (Schwarz and Benzer, 1997) in yellow and the new elements in red.

containing strands A, B, and E and the other containing strands C, D, F, and G (Figures 2A and 2B). With the exception of the long FG loops (residues 468–482 in CBD1 and residues 599–627 in CBD2), the domains are well defined by the ensemble of NMR structures and show good structural statistics (Table 1). Superposition of the central chains of CBD1 and CBD2 (Figure 2C) results in an average rmsd of 1.3 Å (on 101 C$^\alpha$ positions)

with the biggest differences observed for the BC, CD, DE, and the FG loops as well as for parts of the first acidic segment (residues 446–454 and 577–582, respectively). Both domains contain a β bulge in strand A, but only CBD2 displays a second β bulge in strand G. CBD1 instead possesses a *cis* proline at a structurally similar position. Residues Phe376/505, Tyr422/Phe553, Phe431/562, Phe456/587, and Leu460/Ile591 form the core of

Table 1. Experimental NMR Data and Structural Statistics for Ca²⁺ Bound CBD1 and CBD2

	CBD1[a]	CBD2[a]	CBD12
NOE Upper Distance Limits			
Total	2313	2394	4707
Long-range, spanning five or more residues	902	883	1785
Distance Constraint Violations			
Number > 0.3 Å	0	0	4
Maximum	0.15 Å	0.14 Å	0.48 Å
Rmsd	0.015 ± 0.001	0.015 ± 0.001	
TALOS-derived angle constraints	175	186	361
Rmsd	0.62 ± 0.13	0.51 ± 0.28	0.74
PROCHECK Ramachandran Plot Analysis			
Residues in favored regions	84.8%[b]	86.2%[c]	87.7%[b,c]
Residues in additionally allowed regions	14.1%[b]	12.4%[c]	10.9%[b,c]
Residues in generously allowed regions	0.9%[b]	0.9%[c]	0.5%[b,c]
Residues in disallowed regions	0.2%[b]	0.5%[c]	0.9%[b,c]
Rmsd to the Averaged Coordinates			
N, C$^\alpha$, C′	0.66 Å[b]	0.76 Å[c]	
All heavy atoms	1.00 Å[b]	1.19 Å[c]	

[a] Average over the 20 conformers with the lowest NOE energies.
[b] Residues 371–467 and 483–500.
[c] Residues 501–598 and 627–649.

the two domains and are likely to be important for stability.

CBD1 and CBD2 Redefine the Calx-β Motif
Sequence alignments using CBD1 residues 383–460 as a template revealed, amongst others, homology with domains in integrin β4 (Schwarz and Benzer, 1997), extracellular matrix protein 3 (ECM3) of fibers in sea urchins (Hodor et al., 2000), aggregation factor of marine sponges (Fernandez-Busquets et al., 1996), as well as the very large G protein-coupled receptor (VLGR1; [McMillan et al., 2002; Nikkila et al., 2000]) and defined the Calx-β motif (Schwarz and Benzer, 1997). Reexamination of these sequences in view of the CBD1 structure now unequivocally establishes the domain boundaries of this motif and extends it by strands A and G (Figure 2D). Conservation of the structurally important residues and residues involved in Ca²⁺ binding (see below) in the majority of the domains not only suggest preservation of the fold but also that these domains possess very similar ion binding sites. Integrin β4 is special in the sense that all structurally important, but none of the Ca²⁺ coordinating residues, are maintained, hence, raising doubt whether this domain binds Ca²⁺ or any other divalent ions.

Ca²⁺ Binding Sites in CBD1 and CBD2
In order to define the Ca²⁺ binding sites in CBD1 and CBD2, we recorded pseudo-contact shift data, performed structure calculations in the absence of Ca²⁺ ions, and included available mutational data as distance constraints (for details see the Experimental Proce-

dures). This 3-fold approach revealed two Ca²⁺ ions bound within each of the two domains. Unlike for the cadherins, where three Ca²⁺ ions are located above the EF loop and fulfill a purely structural role in the interface of two consecutive extracellular domains (Boggon et al., 2002), Ca²⁺ ions in CBD1 and CBD2 are buried within the domains. The main contributors to the Ca²⁺ binding sites are the two acidic segments Asp446-Glu454 and Asp498-Asp500 in CBD1 (Figures 1B and 3A) as well as Asp577-Glu582 and Glu647-Glu648 in CBD2 (Figures 1B and 3B). In particular, Glu385 located in the AB loop, Asp448 and Glu451 in the first, and Asp498 and Asp500 in the second acidic segment form Ca²⁺ binding site I in CBD1. Opposite to site I, Asp447, Glu451, and Glu454 of the first acidic segment, as well as Asp421 in the CD loop, coordinate the Ca²⁺ in site II. In contrast, CBD2 lacks residues equivalent to Asp448 and Asp500. Instead, Asp578 takes over the role of Asp448 and, similarly to Glu451 in CBD1, coordinates Ca²⁺ ions in both sites. Lys585 in CBD2 occupies a position equivalent to Glu454 in CBD1 and forms a salt bridge with O$^{\delta 1}$ of Asp552 that constitutes an acidic cluster together with Asp578, Glu579, and Glu580. As a consequence of this altered ion coordination in CBD2, its Ca²⁺ ions are shifted by ∼2 Å relative to the Ca²⁺ binding sites in CBD1. With the exception of NCX1 isoforms containing the mutually exclusive exon B, residues contributing to Ca²⁺ binding are highly conserved within the NCX family, thus suggesting similar Ca²⁺ binding properties for all NCXs.

Ca²⁺-Free Forms of CBD1 and CBD2
In order to explore structural effects of Ca²⁺ binding in CBD1 and CBD2, we also recorded [¹H,¹⁵N]-HSQC spectra for the two domains in the presence of 10 mM EDTA. Strikingly, the CBD1 spectrum displayed a strong decrease in peak dispersion with a large number of ¹H resonances clustered in a spectral region, usually characteristic for unstructured residues (Figure S1A available in the Supplemental Data with this article online). Mapping shifted resonances, likely to result from structural alterations or residues exposed to a changed chemical environment (orange) and disappearing resonances, probably reflecting unstructured residues (yellow) onto the molecular structure of CBD1, reveals a loss of structural integrity in the upper half of the molecule (Figure 3C). In particular, residues in the second part of strand A, the initial parts of strands B and F, the end of strand G, as well as the AB, CD, and EF loops, which form the Ca²⁺ binding sites, become unstructured. In sharp contrast, the [¹H,¹⁵N]-HSQC spectrum of CBD (Figure S1B) does not show this degree of chemical shift changes, thus suggesting only limited structural alterations and preservation of the fold in the absence of Ca²⁺. This distinct behavior in the [¹H,¹⁵N]-HSQC spectra of the individual domains in the absence of Ca²⁺ is also observed for CBD12, the construct containing both domains.

Two Distinctly Different Ca²⁺ Sensors
The striking differences observed for CBD1 and CBD2 thus raise the question of their cause and functional consequences. Examination of the CBD1 and CBD2 Ca²⁺ binding sites reveals the presence of three basic residues, Arg547, Lys583, and most importantly Lys585, in CBD2 that are well positioned to form salt bridges with
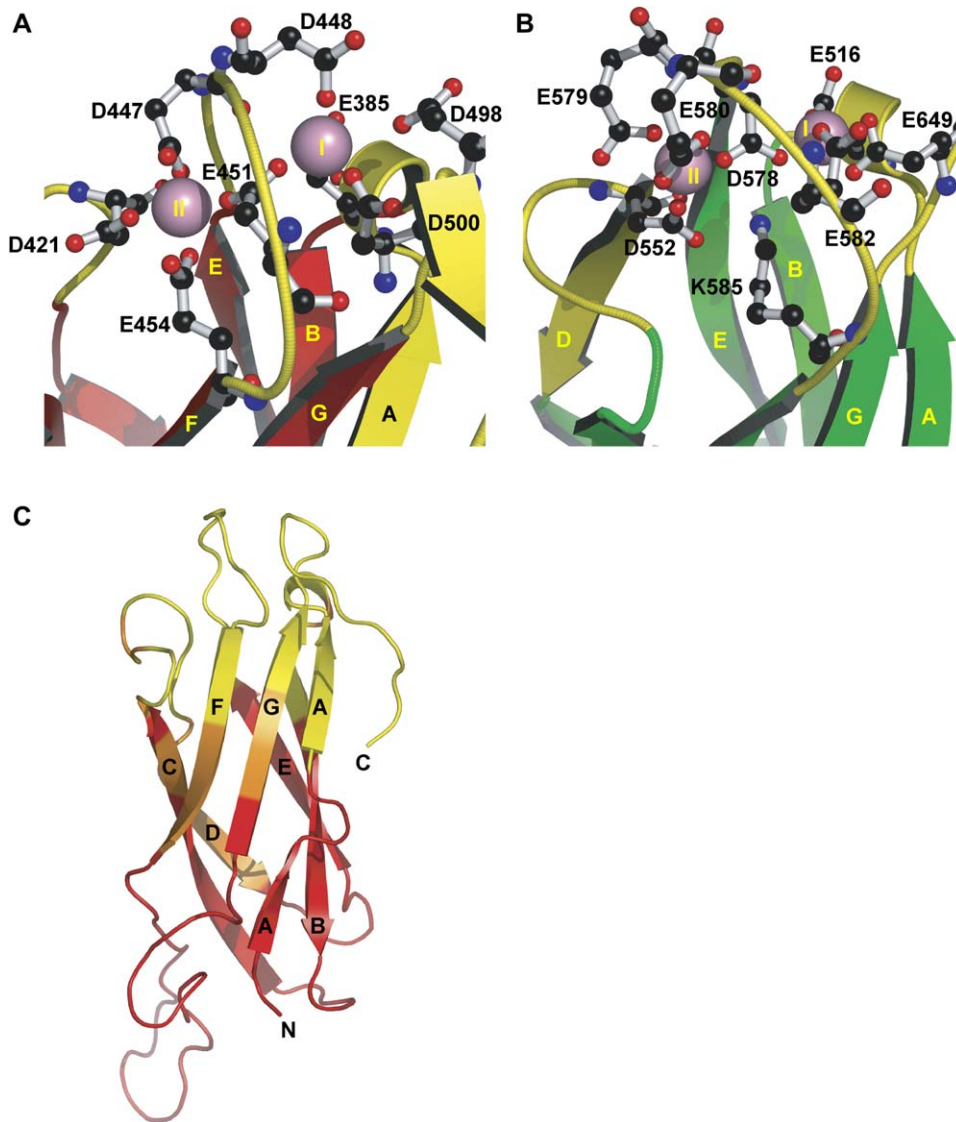
Figure 3. Ca²⁺ Binding in CBD1 and CBD2

(A and B) These panels display Ca²⁺ coordinating residues in CBD1 and CBD2, respectively. Yellow colored ribbons represent residues experiencing pseudo-contact shifts originating from paramagnetic Yb³⁺ ions, whereas unaffected secondary structure elements are given in their unique colors (as defined in Figure 1).

(C) CBD1 chemical shift changes observed between the Ca²⁺-free and bound forms. In red are unchanged resonances, whereas orange and yellow represent strongly shifted and disappearing resonances, respectively.

Glu579, Glu580, and Asp552, respectively (Figure 3B). Upon Ca²⁺ release, these salt bridges in Ca²⁺ binding site II may partly stabilize some of the negative charges and therefore prevent unfolding of CBD2. In sharp contrast, Ca²⁺ binding sites in CBD1 do not contain any basic residues that could reduce repulsion between the numerous glutamate and aspartate residues.

To verify this hypothesis, we aimed to invert the behavior of the two domains by mutating Lys585 in CBD2 to a glutamate and the orthologuous residue in CBD1, Glu454 to a lysine residue. Indeed, contrary to their wild-type forms, [¹H,¹⁵N]-HSQC spectra of the Glu454Lys (Figure S1C) and Lys585Glu (Figure S1D) mutants in the presence of EDTA are characteristic for a fully structured and disintegrated domain, respectively. Likewise, gel

mobility shifts on native polyacrylamide gels in the absence and presence of Ca²⁺ (Figure 4A) are similarly indicative of the dramatic conformational differences. We therefore conclude that electrostatic repulsion is the major driving force for the unfolding of CBD1 in the absence of Ca²⁺.

To further characterize Ca²⁺ binding, we determined dissociation constants of wild-type CBD1 and CBD2 as well as of the Glu454Lys and Lys585Glu mutants by isothermal titration calorimetry (ITC; Figure 4B). The ITC measurements demonstrate that CBD1 binds Ca²⁺ with K_d values of 120 and 240 nM, whereas the respective values of CBD2 are 820 nM and 8.6 μM. Strikingly, the Lys585Glu mutant exhibits for its first Ca²⁺ binding event an affinity comparable to CBD1, whereas the Glu454Lys
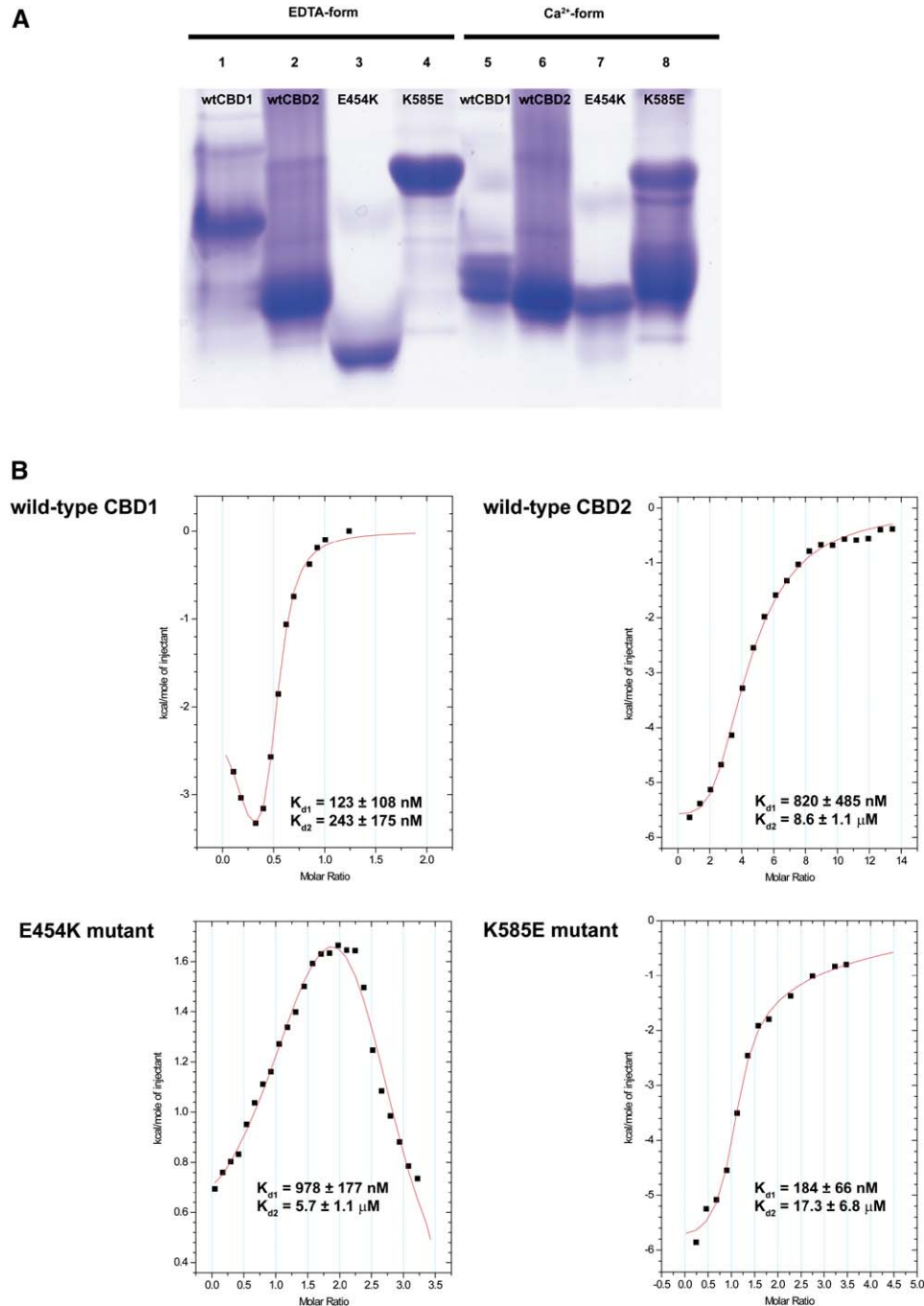
A

B

Figure 4. Biochemical Analyses of Ca^{2+} Binding Sites

(A) Native gel electrophoresis in the absence (lanes 1–4) and presence (lanes 5–8) of Ca^{2+} for wild-type CBD1 and CBD2 as well as the Glu454Lys and Lys585Glu mutants. Although the mobility of CBD2 is largely unchanged under both conditions, CBD1 and K585E show large shifts, indicating substantial conformational changes in their three-dimensional structure. Samples with and without Ca^{2+} contained 10 mM $CaCl_2$ and 10 mM EDTA, respectively, and were incubated for 10 min before loading. Additional minor bands are likely a result of the technical limitations of native gel electrophoresis as only single bands were observed on denaturing gels and only one conformation is observed in the corresponding [^1H,^{15}N]-HSQC spectra under the same conditions.

(B) Isothermal titration calorimetry of Ca^{2+} binding sites in wild-type CBD1 and CBD2, as well as the Glu454Lys and Lys585Glu mutants. ITC curves show heats evolved on adding aliquots of $CaCl_2$.

mutant has attained the binding affinities of CBD2. However, intriguingly, only the Glu454Lys mutant shows an endothermic reaction typical of electrostatic interactions, whereas Ca^{2+} binding in wild-type CBD1, CBD2, and the Lys585Glu mutant is exothermic. Taken together, the NMR, gel mobility shift and ITC data demonstrate that point mutations Glu454Lys and Lys585Glu have very similar properties to CBD2 and CBD1, respectively, and in a way reverse the functionality of their wild-type domains.

Model of the Intact Exchanger

A key aspect of the two Ca²⁺ binding domains is their relative orientation to each other in the regulatory exchanger loop. A first indication of the arrangement between the domains originates from the turn at Asp498 in the CBD1 structure that directs residues 501–509, constituting strand A in CBD2, into an antiparallel orientation with respect to strand G of CBD1 (Figure 3A). Comparison of the [¹H,¹⁵N]-HSQC spectrum of CBD12 with [¹H,¹⁵N]-HSQC spectra of the individual domains in the presence of Ca²⁺ reveals that the majority of the shifting resonances are observed for residues in the Ca²⁺ binding regions of both domains as well as for residues 374–375, 379–382, 490–505, 529–531, 563–566, 598–603, 632–637, and 641. Taking these shifting resonances as ambiguous interaction restraints (in a fashion similar to the HADDOCK approach [Dominguez et al., 2003]) in combination with restrictions imposed by the orientation of Asp499-Ala502, we obtained a model for CBD12 that was eventually refined in explicit water (Figure 5A and Table 1). This model displays an antiparallel arrangement of the Ca²⁺ binding domains with an extensive network of interactions in the center between residues in and around the β bulges in strand A of CBD1 and strand G in CBD2.

In order to interpret Ca²⁺ binding and release events in the context of the intact NCX, we also constructed a hypothetical model for the entire exchanger with a simplified version displayed in Figure 5B (for details on the intact exchanger model, see the Supplemental Data). Based on a homology we found with α-catenin (PDB code 1H6G; Yang et al., 2001), we propose that the remainder of the regulatory loop (residues 217–370 and 651–705) forms a third domain, which we designate as CLD or catenin-like domain. Furthermore, as a consequence of sequence conservation with P type ATPases (Nicoll et al., 1990; Ogawa and Toyoshima, 2002), we suggest that residues Val194, Val195, Val197, and Glu199 in NCX constitute a large part of the transport Ca²⁺ binding site within the TM. In this model, the Ca²⁺ binding sites of CBD1 are ~90 Å away from the transport Ca²⁺ binding site, whereas cassette exons C–F in CBD2 are located directly opposite to the CBD1 Ca²⁺ binding sites. In contrast, the CBD2 Ca²⁺ binding sites must be in close proximity to the CLD, the region suggested to be responsible for Na⁺-dependent exchanger inactivation.

Effects of Alternative Splicing and Phosphorylation

Analysis of a large number of cell types expressing spliced isoforms reveals exon A to be exclusively expressed in excitable tissues such as heart and skeletal muscle as well as neuronal tissues where rapid and substantial Ca²⁺ fluxes are important in signaling pathways (Qiu et al., 2001). In strong contrast to this, isoforms containing exon B are only found in nonexcitable tissues (Quednau et al., 1997). Furthermore, giant excised patch clamp experiments demonstrated that exon A containing NCX1 isoforms, in contrast to exon B containing variants, can alleviate intracellular Na⁺-dependent inactivation (Dyck et al., 1999). Interestingly, exons A and B encode the first acidic segment of the Ca²⁺ binding sites in CBD2 (Figures 1B and 3B), and substitution of Asp578 by an arginine residue (as in exon B) appears to be sufficient to prevent alleviation of Na⁺-dependent exchanger

inactivation (Dunn et al., 2002). As Asp578 coordinates Ca²⁺ ions in both sites in CBD2, substitution by an arginine residue may be especially detrimental due to the introduction of a positive charge into the highly negative environment. In exon B variants, this may result in partial destruction or rearrangement of the ion binding sites that could alter the interaction with the CLD and therefore renders overcoming of Na⁺-dependent inactivation impossible.

On the other side of CBD2, juxtaposition of cassette exons C, D, E, and F to the CBD1 Ca²⁺ binding sites (Figures 5A and 5B) may enable splice variants to modulate effects induced by Ca²⁺ binding and thereby adjust Na⁺/Ca²⁺ exchange to special needs. For instance, *Drosophila* splice variants CalX1.1 and CalX1.2, which only differ in five amino acids, exhibit significant differences in their Na⁺- and Ca²⁺-dependent regulatory properties (Omelchenko et al., 1998). The corresponding residues in canine NCX1, Ser600-Gly604, display chemical shift changes in the [¹H,¹⁵N]-HSQC spectrum of CBD12 compared to the individual CBD2 spectrum, indicating an interaction between these residues and the CBD1 Ca²⁺ binding sites. Another example for Na⁺/Ca²⁺ exchange modulation originates from frog heart, where an additional 9-amino acid exon after exon E (Figure 1B) is predicted to generate an ATP/GTP binding motif that renders the molecule regulatable by cAMP (Shuba et al., 1998). Intriguingly, in the CBD2 structure, residues 604–623 are disordered as also confirmed by ¹⁵N dynamics measurements that yielded {¹⁵N-¹H}-NOE values < 0.7. However, this region may rigidify in other splice variants or upon binding of the nucleotide in the frog exchanger. Alternatively, the exposed position of the cassette exons may also permit an indirect modulation through an interaction with other proteins.

Finally, in the center of the first acidic segment, Phe450 and its counterpart Tyr581 in CBD2 seem to occupy an unusual, solvent-exposed position (Figure 2C). Although the presence of Phe450 at this position is unclear, Tyr581 is a potential substrate for protein tyrosine kinases (Quednau et al., 1997). Phosphorylation of Tyr581 would bring additional negative charges into the proximity of at least one Ca²⁺ binding site and would likely have a profound effect on ion binding.

Function of the Disordered CBD1 FG Loop in the Intact Enzyme

The *Drosophila* exchanger CalX1.1 is unique among characterized members of the exchanger family in that μM levels of Ca²⁺ rather inhibit than activate ion-exchange across the plasma membrane (Hryshko et al., 1996). Interestingly, a CalX1.1 chimera with Lys404-Tyr580 replaced by the corresponding residues Leu336-Thr528 of cardiac NCX1 restored the positive regulatory response to Ca²⁺ (Dyck et al., 1998). The only obvious difference between the sequences in the chimeric region is the absence of NCX1 residues 469–485 in CalX1.1 that correspond to large parts of the FG loop in CBD1, therefore suggesting involvement of the FG loop in Ca²⁺-dependent exchanger activation. Additional support for the relevance of the FG loop arises from calpain cleavages in the same region of CBD1 for NCX1 and NCX3 that inactivate these exchanger isoforms and eventually result in cell death as a consequence of Ca²⁺ overload (Bano et al., 2005). Although spectra of the CBD1
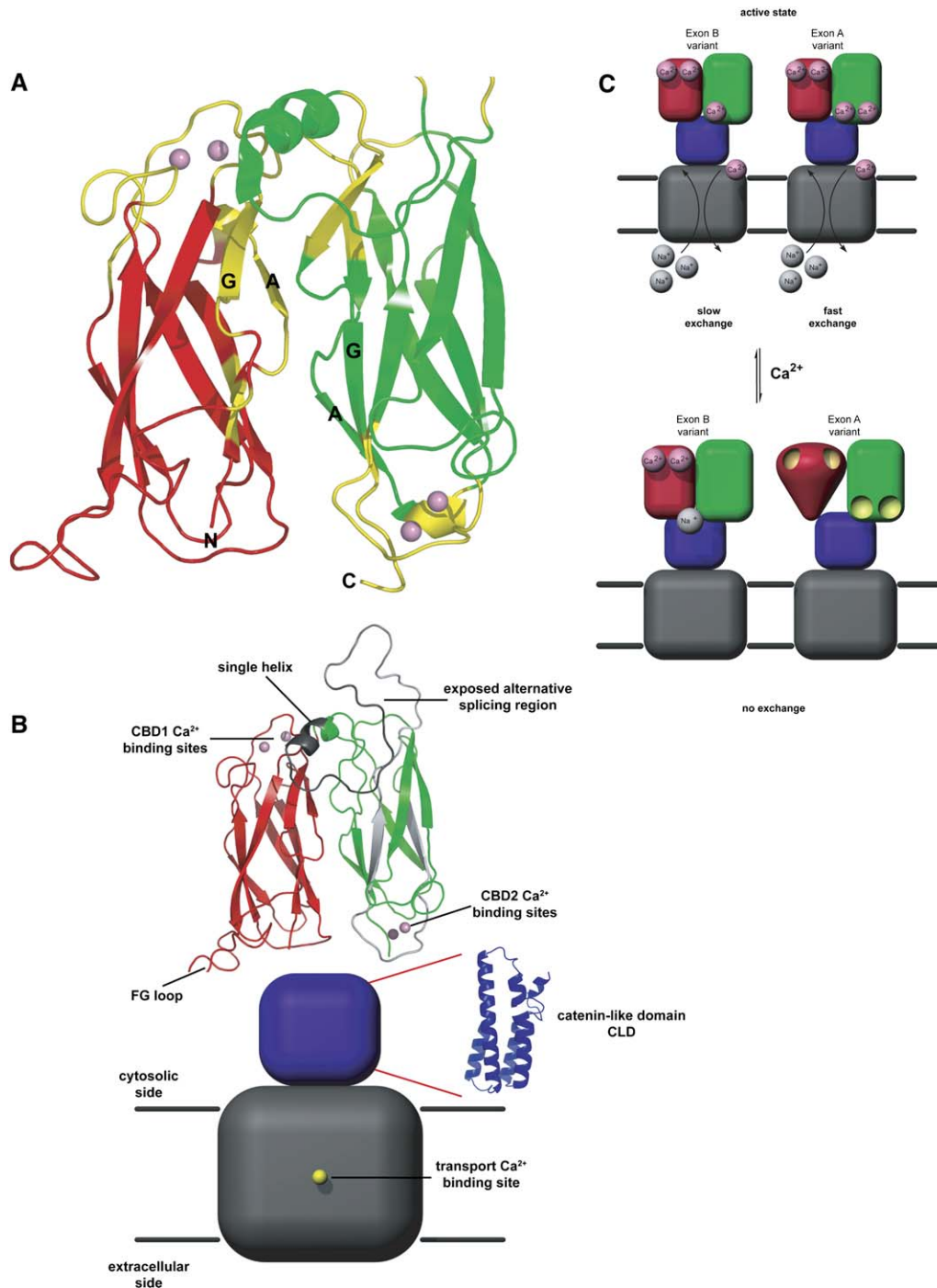
Figure 5. Model of the Intact Exchanger

(A) Blow-up view of the interface between CBD1 and CBD2. Residues that display chemical shift changes in the [^{1}H,^{15}N]-HSQC spectrum of CBD12 are colored yellow.

(B) Hypothetical model of the intact exchanger that is composed of CBD1 (red), CBD2 (green), CLD (blue), and the TM (gray). Exons A and D are colored in light and dark gray, respectively.

(C) Schematic outline of exchanger operation. NCX is initially activated by the large conformational change resulting from binding of Ca^{2+} ions to CBD1 (red) and may undergo faster turnovers at high intracellular Ca^{2+} concentrations when the CBD2 Ca^{2+} binding sites (green; exon A containing variants) become occupied. Variants containing exon A are able to alleviate Na$^+$-dependent exchanger inactivation and become inactivated by Ca^{2+} release from the CBD1 binding sites. Exon B containing variants can be inactivated through binding of Na$^+$ ions even Ca^{2+} ions are bound to the CBD1 binding sites.

construct suggest the FG loop to be unstructured in the individual domain, in our model for the complete intracellular exchanger loop, hydrophobic patches on the CLD, located opposite to Val480, Ala482, Leu483, Ala484, and Leu485, could stabilize the FG loop in the intact NCX.

Conclusions

Our study revealed the existence of three domains in the large intracellular loop of NCX. The two consecutive Ca^{2+} binding domains CBD1 and CBD2 are arranged in an antiparallel fashion and are connected via a third domain that we designated as CLD (Figure 5B and Figure S2) to the membrane part of the exchanger. Mutually exclusive exons A or B as well as cassette exons C–F in CBD2 are ideally positioned to modulate Na^+/Ca^{2+} exchange in order to satisfy needs at different places in the cell or cells in different tissues.

During the course of a typical Ca^{2+} transient in the cell, NCX in concert with the plasma membrane/sarcoplasmic Ca^{2+} ATPases and the mitochondrial uniporter remove Ca^{2+} from the cytoplasm and maintain the resting level of Ca^{2+} at ~100 nM (Carafoli, 2002; Berridge et al., 2003). In this process, CBD1 as the primary Ca^{2+} sensor in NCX (Figure 5C) detects the slightest increase in cytosolic Ca^{2+} and the associated, large structural changes activate the exchanger. In contrast, CBD2 undergoes comparably modest structural alterations and binds Ca^{2+} only at elevated Ca^{2+} concentrations. These two different sensitivity thresholds may enable NCX to function dynamically over a wide range of Ca^{2+} concentrations and permit high Ca^{2+} fluxes in excitable cells.

Experimental Procedures

Sample Preparation

Nucleotide sequences encoding residues 371–509, 501–657, and 371–657 of canine NCX1 (accession code P23685; AD-splice variant) were cloned into a pET23b vector and expressed in *E. coli* BL21(DE3) at 37ºC for ~5 hr by using 1 mM IPTG for induction. Purification was facilitated by N-terminal His tags and anion-exchange chromatography (MonoQ, Amersham-Pharmacia). Purity of all samples was >95% as judged by SDS-PAGE and [^{1}H,^{15}N]-HSQC spectra. Ca^{2+} bound NMR samples used for structure determination contained uniformly ^{15}N or ^{15}N/^{13}C labeled protein (0.5–1.0 mM) in 20 mM HEPES (pH 7.0), 20 mM β-mercaptoethanol, and 10 mM CaCl$_2$ buffer and were prepared in H$_2$O/D$_2$O (95%/5%) with 0.02% (w/v) NaN$_3$ as a preservative.

NMR Spectroscopy

NMR spectra of CBD1 and CBD2 were acquired at 33ºC on Varian Inova 600 and 800 MHz spectrometers. Backbone and side chain assignments were obtained employing triple-resonance experiments using standard protocols (Kanelis et al., 2001) and are 94% complete for both domains. The [^{1}H,^{15}N]-HSQC spectrum of CBD12 was recorded from an ~0.3 mM uniformly ^{15}N labeled sample in H$_2$O/D$_2$O (95%/5% [v/v]). Distance restraints for structure calculations were obtained from 3D-^{13}C-NOESY-HSQC and 3D-^{15}N-NOESY-HSQC spectra. All NOESY spectra were measured with an 80 ms NOE-mixing time. Stereospecific assignments of valine and leucine methyl groups were obtained by analysis of [^{1}H,^{13}C] CT-HSQC spectra recorded from 10% ^{13}C labeled samples (Neri et al., 1989). All data were processed with the NMRPipe program suite (Delaglio et al., 1995) and analyzed with the programs XEASY (Bartels et al., 1995) and SPARKY (Goddard and Kneller, University of California, San Francisco).

Structure Calculations

The program TALOS (Cornilescu et al., 1999) was used to generate 175 and 186 ϕ,ψ angle constraints from chemical shifts of CBD1 and CBD2, respectively. For structure determination of CBD1, NOESY cross peaks were manually picked and integrated in the aforementioned NOESY spectra and assigned by using the automated NOESY cross peak assignment method CANDID (Herrmann et al., 2002a) in the program CYANA 2.0 (Güntert et al., 1997). For CBD2, we initially used the program RADAR (Herrmann et al., 2002b). CBD1 and CBD2 NOE peak lists were then manually extended. Finally, a set of the best 100 CYANA conformers was refined in explicit solvent (Spronk et al., 2002) by using the program Xplor-NIH (Schwieters et al., 2003), and the 20 conformers with the lowest NOE energies were selected. The input data and final structures were validated with the programs WHAT_CHECK (Hooft et al., 1996) and PROCHECK-NMR (Laskowski et al., 1996). Figures were generated with MOLSCRIPT (Kraulis, 1991) and PYMOL (DeLano, 2002, http://www.pymol.org).

Elucidation of the Ca2+ Binding Sites

In order to define the Ca^{2+} binding sites in CBD1 and CBD2, we followed a 3-fold approach. First, we recorded [^{1}H,^{15}N]-HSQC spectra in the presence of Yb^{3+} and compared them with the same spectra recorded in the presence of Ca^{2+}. Disappearing or strongly shifted resonances experienced pseudo-contact shifts as a consequence of the paramagnetic properties of Yb^{3+} and involve residues within ~10 Å of the lanthanide. Second, we examined the ensemble of structures that were exclusively derived from NOE and angle constraints in the absence of Ca^{2+} ions. These structures displayed close proximity of acidic residues that would experience strong repulsion in the absence of Ca^{2+}, thus identifying them as potential Ca^{2+} coordinating residues. Third, we used the knowledge obtained from mutational studies, which showed that point mutations for Asp447, Asp448, Asp498, and Asp500 almost entirely abolish Ca^{2+} binding (Levitsky et al., 1994). Using a stepwise approach, we successively included for each residue distance constraints to the Ca^{2+} ions (lower bound 1.7 Å and upper bound 2.8 Å, respectively).

ITC

Prior to concentration, all protein samples were dialyzed against 10 mM EDTA and thereafter thoroughly washed with 20 mM HEPES (Sigma, Ultrapure; pH 7.0), 20 mM β-mercaptoethanol, and 0.2% NaN$_3$ containing buffer in order to remove any contaminating divalent ions. Protein concentrations were determined by UV spectroscopy. Metal salts were prepared in the same buffer at the desired concentrations. ITC experiments were carried out by using a VP-ITC (Microcal LLC) device with typically 5–35 μM buffered protein solution and were repeated at least twice. After thermal equilibration at 25ºC and an initial 2 min delay, 26 serial injections of 10 μl at 300 rpm stirring speed were performed every 5 min. In order to correct the experimental binding isotherm for background heat effects, we also titrated CaCl$_2$ containing buffer into buffer. In line with our experimental structures and the fact that CBD1 and the Glu454Lys mutant titrations cannot be fit with the "one set of sites" model, all corrected curves were fit by using the "two sets of sites" model in the Origin 5.0 software (Microcal LLC). A representative measurement for each titration is shown in Figure 4B.

Supplemental Data

Supplemental Data include Supplemental Experimental Procedures, Supplemental References, and two figures and can be found with this article online at http://www.molecule.org/cgi/content/full/22/1/15/DC1/.

References

Bano, D., Young, K.W., Guerin, C.J., Lefeuvre, R., Rothwell, N.J., Naldini, L., Rizzuto, R., Carafoli, E., and Nicotera, P. (2005). Cleavage of the plasma membrane Na+/Ca2+ exchanger in excitotoxicity. Cell *120*, 275–285.

Bartels, C., Xia, T.H., Billeter, M., Güntert, P., and Wüthrich, K. (1995). The program XEASY for computer-supported NMR spectral analysis of biological macromolecules. J. Biomol. NMR *6*, 1–10.

Berridge, M.J., Bootman, M.D., and Roderick, H.L. (2003). Calcium signalling: dynamics, homeostasis and remodelling. Nat. Rev. Mol. Cell Biol. *4*, 517–529.

Boggon, T.J., Murray, J., Chappuis-Flament, S., Wong, E., Gumbiner, B.M., and Shapiro, L. (2002). C-cadherin ectodomain structure and implications for cell adhesion mechanisms. Science *296*, 1308–1313.

Cai, X., and Lytton, J. (2004). The cation/Ca2+ exchanger super-family: phylogenetic analysis and structural implications. Mol. Biol. Evol. *21*, 1692–1703.

Carafoli, E. (2002). Calcium signaling: a tale for all seasons. Proc. Natl. Acad. Sci. USA *99*, 1115–1122.

Carafoli, E. (2004). Calcium-mediated cellular signals: a story of failures. Trends Biochem. Sci. *29*, 371–379.

Cornilescu, G., Delaglio, F., and Bax, A. (1999). Protein backbone angle restraints from searching a database for chemical shift and sequence homology. J. Biomol. NMR *13*, 289–302.

Delaglio, F., Grzesiek, S., Vuister, G.W., Zhu, G., Pfeifer, J., and Bax, A. (1995). NMRPipe: a multidimensional spectral processing system based on UNIX pipes. J. Biomol. NMR *6*, 277–293.

DeLano, W.L. (2002). The PyMOL Molecular Graphics System (San Carlos, California: Delano Scientific).

Dominguez, C., Boelens, R., and Bonvin, A.M. (2003). HADDOCK: a protein-protein docking approach based on biochemical or biophysical information. J. Am. Chem. Soc. *125*, 1731–1737.

Dunn, J., Elias, C.L., Le, H.D., Omelchenko, A., Hryshko, L.V., and Lytton, J. (2002). The molecular determinants of ionic regulatory differences between brain and kidney Na+/Ca2+ exchanger (NCX1) isoforms. J. Biol. Chem. *277*, 33957–33962.

Dyck, C., Maxwell, K., Buchko, J., Trac, M., Omelchenko, A., Hnato-wich, M., and Hryshko, L.V. (1998). Structure-function analysis of CALX1.1, a Na+-Ca2+ exchanger from Drosophila. Mutagenesis of ionic regulatory sites. J. Biol. Chem. *273*, 12981–12987.

Dyck, C., Omelchenko, A., Elias, C.L., Quednau, B.D., Philipson, K.D., Hnatowich, M., and Hryshko, L.V. (1999). Ionic regulatory properties of brain and kidney splice variants of the NCX1 Na+-Ca(2+) exchanger. J. Gen. Physiol. *114*, 701–711.

Egger, M., and Niggli, E. (1999). Regulatory function of Na-Ca exchange in the heart: milestones and outlook. J. Membr. Biol. *168*, 107–130.

Fernandez-Busquets, X., Kammerer, R.A., and Burger, M.M. (1996). A 35-kDa protein is the basic unit of the core from the 2 x 10(4)-kDa aggregation factor responsible for species-specific cell adhesion in the marine sponge Microciona prolifera. J. Biol. Chem. *271*, 23558–23565.

Güntert, P., Mumenthaler, C., and Wüthrich, K. (1997). Torsion angle dynamics for NMR structure calculation with the new program DYANA. J. Mol. Biol. *273*, 283–298.

Herrmann, T., Güntert, P., and Wüthrich, K. (2002a). Protein NMR structure determination with automated NOE assignment using the new software CANDID and the torsion angle dynamics algorithm DYANA. J. Mol. Biol. *319*, 209–227.

Herrmann, T., Güntert, P., and Wüthrich, K. (2002b). Protein NMR structure determination with automated NOE-identification in the NOESY spectra using the new software ATNOS. J. Biomol. NMR *24*, 171–189.

Hilgemann, D.W. (1990). Regulation and deregulation of cardiac Na(+)-Ca2+ exchange in giant excised sarcolemmal membrane patches. Nature *344*, 242–245.

Hilgemann, D.W., Nicoll, D.A., and Philipson, K.D. (1991). Charge movement during Na+ translocation by native and cloned cardiac Na+/Ca2+ exchanger. Nature *352*, 715–718.

Hilgemann, D.W., Collins, A., and Matsuoka, S. (1992a). Steady-state and dynamic properties of cardiac sodium-calcium exchange. Secondary modulation by cytoplasmic calcium and ATP. J. Gen. Physiol. *100*, 933–961.

Hilgemann, D.W., Matsuoka, S., Nagel, G.A., and Collins, A. (1992b). Steady-state and dynamic properties of cardiac sodium-calcium exchange. Sodium-dependent inactivation. J. Gen. Physiol. *100*, 905–932.

Hodor, P.G., Illies, M.R., Broadley, S., and Ettensohn, C.A. (2000). Cell-substrate interactions during sea urchin gastrulation: migrating primary mesenchyme cells interact with and align extracellular matrix fibers that contain ECM3, a molecule with NG2-like and multiple calcium-binding domains. Dev. Biol. *222*, 181–194.

Hooft, R.W.W., Vriend, G., Sander, C., and Abola, E.E. (1996). Errors in protein structures. Nature *381*, 272.

Hryshko, L.V., Matsuoka, S., Nicoll, D.A., Weiss, J.N., Schwarz, E.M., Benzer, S., and Philipson, K.D. (1996). Anomalous regulation of the Drosophila Na(+)-Ca2+ exchanger by Ca2+. J. Gen. Physiol. *108*, 67–74.

Iwamoto, T., and Shigekawa, M. (1998). Differential inhibition of Na+/Ca2+ exchanger isoforms by divalent cations and isothiourea derivative. Am. J. Physiol. *275*, C423–C430.

Iwamoto, T., Nakamura, T.Y., Pan, Y., Uehara, A., Imanaga, I., and Shigekawa, M. (1999). Unique topology of the internal repeats in the cardiac Na+/Ca2+ exchanger. FEBS Lett. *446*, 264–268.

Kanelis, V., Forman-Kay, J.D., and Kay, L.E. (2001). Multidimensional NMR methods for protein structure determination. IUBMB Life *52*, 291–302.

Kang, T.M., and Hilgemann, D.W. (2004). Multiple transport modes of the cardiac Na+/Ca2+ exchanger. Nature *427*, 544–548.

Kirichok, Y., Krapivinsky, G., and Clapham, D.E. (2004). The mito-chondrial calcium uniporter is a highly selective ion channel. Nature *427*, 360–364.

Kofuji, P., Lederer, W.J., and Schulze, D.H. (1994). Mutually exclusive and cassette exons underlie alternatively spliced isoforms of the Na/Ca exchanger. J. Biol. Chem. *269*, 5145–5149.

Kraulis, P.J. (1991). MOLSCRIPT: a program to produce both detailed and schematic plots on protein structures. J. Appl. Crystallogr. *24*, 946–950.

Laskowski, R.A., Rullmannn, J.A., MacArthur, M.W., Kaptein, R., and Thornton, J.M. (1996). AQUA and PROCHECK-NMR: programs for checking the quality of protein structures solved by NMR. J. Biomol. NMR *8*, 477–486.

Lee, S.L., Yu, A.S., and Lytton, J. (1994). Tissue-specific expression of Na(+)-Ca2+ exchanger isoforms. J. Biol. Chem. *269*, 14849–14852.

Levitsky, D.O., Nicoll, D.A., and Philipson, K.D. (1994). Identification of the high affinity Ca(2+)-binding domain of the cardiac Na(+)-Ca2+ exchanger. J. Biol. Chem. *269*, 22847–22852.

Li, Z., Matsuoka, S., Hryshko, L.V., Nicoll, D.A., Bersohn, M.M., Burke, E.P., Lifton, R.P., and Philipson, K.D. (1994). Cloning of the NCX2 isoform of the plasma membrane Na(+)-Ca2+ exchanger. J. Biol. Chem. *269*, 17434–17439.

Linck, B., Qiu, Z., He, Z., Tong, Q., Hilgemann, D.W., and Philipson, K.D. (1998). Functional comparison of the three isoforms of the Na+/Ca2+ exchanger (NCX1, NCX2, NCX3). Am. J. Physiol. *274*, C415–C423.

Marshall, C.R., Fox, J.A., Butland, S.L., Ouellette, B.F., Brinkman, F.S., and Tibbits, G.F. (2005). Phylogeny of Na+-Ca2+ Exchanger (NCX) genes from genomic data identifies new gene duplications and a new family member in fish species. Physiol. Genomics *21*, 161–173.

Matsuoka, S., Nicoll, D.A., Reilly, R.F., Hilgemann, D.W., and Philipson, K.D. (1993). Initial localization of regulatory regions of the

cardiac sarcolemmal Na(+)-Ca2+ exchanger. Proc. Natl. Acad. Sci. USA *90*, 3870–3874.

McMillan, D.R., Kayes-Wandover, K.M., Richardson, J.A., and White, P.C. (2002). Very large G protein-coupled receptor-1, the largest known cell surface protein, is highly expressed in the developing central nervous system. J. Biol. Chem. *277*, 785–792.

Neri, D., Szyperski, T., Otting, G., Senn, H., and Wüthrich, K. (1989). Stereospecific nuclear magnetic resonance assignments of the methyl groups of valine and leucine in the DNA-binding domain of the 434 repressor by biosynthetically directed fractional 13C labeling. Biochemistry *28*, 7510–7516.

Nicoll, D.A., Longoni, S., and Philipson, K.D. (1990). Molecular cloning and functional expression of the cardiac sarcolemmal Na(+)-Ca2+ exchanger. Science *250*, 562–565.

Nicoll, D.A., Hryshko, L.V., Matsuoka, S., Frank, J.S., and Philipson, K.D. (1996a). Mutation of amino acid residues in the putative transmembrane segments of the cardiac sarcolemmal Na+-Ca2+ exchanger. J. Biol. Chem. *271*, 13385–13391.

Nicoll, D.A., Quednau, B.D., Qui, Z., Xia, Y.R., Lusis, A.J., and Philipson, K.D. (1996b). Cloning of a third mammalian Na+-Ca2+ exchanger, NCX3. J. Biol. Chem. *271*, 24914–24921.

Nicoll, D.A., Ottolia, M., Lu, L., Lu, Y., and Philipson, K.D. (1999). A new topological model of the cardiac sarcolemmal Na+-Ca2+ exchanger. J. Biol. Chem. *274*, 910–917.

Nikkila, H., McMillan, D.R., Nunez, B.S., Pascoe, L., Curnow, K.M., and White, P.C. (2000). Sequence similarities between a novel putative G protein-coupled receptor and Na+/Ca2+ exchangers define a cation binding domain. Mol. Endocrinol. *14*, 1351–1364.

Ogawa, H., and Toyoshima, C. (2002). Homology modeling of the cation binding sites of Na+K+-ATPase. Proc. Natl. Acad. Sci. USA *99*, 15977–15982.

Omelchenko, A., Dyck, C., Hnatowich, M., Buchko, J., Nicoll, D.A., Philipson, K.D., and Hryshko, L.V. (1998). Functional differences in ionic regulation between alternatively spliced isoforms of the Na+-Ca2+ exchanger from Drosophila melanogaster. J. Gen. Physiol. *111*, 691–702.

Ottolia, M., Philipson, K.D., and John, S. (2004). Conformational changes of the Ca(2+) regulatory site of the Na(+)-Ca(2+) exchanger detected by FRET. Biophys. J. *87*, 899–906.

Qiu, Z., Nicoll, D.A., and Philipson, K.D. (2001). Helix packing of functionally important regions of the cardiac Na(+)-Ca(2+) exchanger. J. Biol. Chem. *276*, 194–199.

Quednau, B.D., Nicoll, D.A., and Philipson, K.D. (1997). Tissue specificity and alternative splicing of the Na+/Ca2+ exchanger isoforms NCX1, NCX2, and NCX3 in rat. Am. J. Physiol. *272*, C1250–C1261.

Schwarz, E.M., and Benzer, S. (1997). Calx, a Na-Ca exchanger gene of Drosophila melanogaster. Proc. Natl. Acad. Sci. USA *94*, 10249–10254.

Schwieters, C.D., Kusyewski, J.J., Tjandra, N., and Clore, G.M. (2003). The Xplor-NIH NMR molecular structure determination package. J. Magn. Reson. *160*, 66–74.

Shuba, Y.M., Iwata, T., Naidenov, V.G., Oz, M., Sandberg, K., Kraev, A., Carafoli, E., and Morad, M. (1998). A novel molecular determinant for cAMP-dependent regulation of the frog heart Na+-Ca2+ exchanger. J. Biol. Chem. *273*, 18819–18825.

Spronk, C.A., Linge, J.P., Hilbers, C.W., and Vuister, G.W. (2002). Improving the quality of protein structures derived by NMR spectroscopy. J. Biomol. NMR *22*, 281–289.

Wang, T., Xu, H., Oberwinkler, J., Gu, Y., Hardie, R.C., and Montell, C. (2005). Light activation, adaptation, and cell survival functions of the Na+/Ca2+ exchanger CalX. Neuron *45*, 367–378.

Yang, J., Dokurno, P., Tonks, N.K., and Barford, D. (2001). Crystal structure of the M-fragment of alpha-catenin: implications for modulation of cell adhesion. EMBO J. *20*, 3645–3656.

Accession Numbers